HHS Public Access

Author manuscript

J Immunol. Author manuscript; available in PMC 2020 December 01.

Published in final edited form as:

J Immunol. 2019 December 01; 203(11): 2827–2836. doi:10.4049/jimmunol.1801338.

UBASH3A regulates the synthesis and dynamics of T-cell receptor-CD3 complexes

Yan Ge[*,†], **Taylor K. Paisie**[*,†,‡], **Sixue Chen**[†,‡,§,¶,‖], **Patrick Concannon**[*,†]

[*]Department of Pathology, Immunology and Laboratory Medicine, University of Florida, Gainesville, FL 32610

[†]Genetics Institute, University of Florida, Gainesville, FL 32610

[‡]Genetics & Genomics Graduate Program, University of Florida, Gainesville, FL 32610

[§]Department of Biology, University of Florida, Gainesville, FL 32611

[¶]Plant Molecular and Cellular Biology Program, University of Florida, Gainesville, FL 32611

[‖]Interdisciplinary Center for Biotechnology Research, University of Florida, Gainesville, FL 32610

Abstract

The T-cell receptor (TCR)-CD3 complex is a multicomponent membrane receptor, the expression of which is tightly regulated in thymocytes, as well as in mature T cells both at steady state and upon stimulation. Here, we report novel roles for UBASH3A (Ubiquitin-associated and SH3 containing A) in TCR-CD3 synthesis and turnover. UBASH3A is a negative regulator of T-cell function, and plays a broad role in autoimmunity. We show that modulation of UBASH3A levels in unstimulated Jurkat cells leads to altered amounts of total cellular CD3 chains and of cell-surface TCR-CD3 complexes; in contrast, UBASH3A does not affect the level of cell-surface CD28, an important T-cell costimulatory receptor. Upon TCR engagement, UBASH3A enhances the downmodulation of cell-surface TCR-CD3. Mass spectrometry and protein-protein interaction studies uncover novel associations between UBASH3A and components of several cellular pathways involved in the regulation of TCR-CD3 turnover and dynamics, including ER-associated protein degradation (ERAD), cell motility, endocytosis and endocytic recycling of membrane receptors. Finally, we demonstrate that the SH3 domain of UBASH3A mediates its binding to CBL-B, an E3 ubiquitin ligase which negatively regulates CD28-mediated signaling and hence T-cell activation. In summary, this study provides new mechanistic insights into how UBASH3A regulates T-cell activation and contributes to autoimmunity. The interaction between UBASH3A and CBL-B may synergistically inhibit T-cell function, and affect risk for type 1 diabetes as both genes have been shown to be associated with this autoimmune disease.

Address correspondence and reprint requests to Dr. Yan Ge or Dr. Patrick Concannon, Department of Pathology, Immunology and Laboratory Medicine, University of Florida, 2033 Mowry Road, CGRC Room 430G, Gainesville, FL 32610 (Y.G.) or Department of Pathology, Immunology and Laboratory Medicine, University of Florida, 2033 Mowry Road, CGRC Room 115, Gainesville, FL 32610 (P.C.). Telephone: (352) 273-8290, Fax: (352) 273-8284, yange09@ufl.edu (Y.G.) or patcon@ufl.edu (P.C.).

Y.G. and P.C. conceived the study, interpreted the data, and wrote the manuscript. Y.G. and T.K.P. performed the experiments. Y.G. analyzed the data. S.C. assisted in the design and analysis of the mass spectrometry experiments.

Introduction

UBASH3A (also known as STS-2, TULA, and CLIP4) is a negative regulator of T-cell activation and function (1–6). Genetic variants in *UBASH3A* have been associated with at least five distinct autoimmune diseases (7–18), suggesting a broad role of *UBASH3A* in autoimmunity.

UBASH3A is expressed primarily in T cells and encodes a protein called ubiquitin-associated and SH3 domain containing A (1, 3, 5). In mice, *Ubash3a* mRNA is also detected in the thymus, suggesting a role in T-cell development (1). The T-cell-specific expression pattern of *UBASH3A* distinguishes it from its ubiquitously expressed paralogue, *UBASH3B* (also known as *STS-1* and *TULA-2*). Unlike *UBASH3A*, *UBASH3B* has not been associated with any autoimmune disease in genome-wide association studies.

UBASH3A has three structural domains: the N-terminal UBA (ubiquitin-associated), SH3 (Src homology 3), and the C-terminal histidine phosphatase (also referred to as phosphoglycerate mutase-like, PGM) domains. The UBA domain can bind to mono-ubiquitin as well as lysine-63- and methionine-1-linked polyubiquitin chains (5, 19). UBASH3A has four identified ubiquitination sites at lysine residues 15, 202, 309 and 358. Monoubiquitination at Lys 202 causes UBASH3A to adopt a closed conformation, which prevents the binding of the UBA domain to substrates *in trans* (19). The SH3 domain interacts with dynamin (20), which is required for endocytosis; and with CBL (21, 22), an E3 ubiquitin ligase. The PGM domain mediates self-dimerization (23). Despite structural similarity, the PGM domain of UBASH3A exhibits only very weak, possibly acid-dependent, phosphatase activity (2, 24), compared to UBASH3B, which has readily demonstrable phosphatase activity *in vitro*, and suppresses T-cell receptor (TCR) signaling *in vivo* by dephosphorylating ZAP-70 and Syk, two key molecules involved in the amplification of TCR-triggered signals (2, 25–28).

Mice lacking either *Ubash3a* (*Ubash3a*$^{-/-}$) or *Ubash3b* (*Ubash3b*$^{-/-}$) or both paralogues (*Ubash3a*$^{-/-}$*Ubash3b*$^{-/-}$) have been constructed, but none of these lines exhibit overt defects in the absence of immune challenge (1). Upon TCR stimulation, isolated *Ubash3a*$^{-/-}$*Ubash3b*$^{-/-}$ T cells are hyper-proliferative and produce more IL-2 and IFNγ than wild-type T cells, while T cells from *Ubash3a*$^{-/-}$ and *Ubash3b*$^{-/-}$ single-knockout mice display only a modest increase in proliferation (2). Consistent with its negligible phosphatase activity, the knockout of *Ubash3a* alone results in only a slight increase in phosphorylation of ZAP-70 (2). Thus, in mice, while *Ubash3a* does act, in combination with *Ubash3b*, to suppress T-cell signaling, the primary source of the phosphatase activity for this role is *Ubash3b* (1–4).

We previously reported that UBASH3A attenuates NF-κB signaling by inhibiting the activation of the IκB kinase complex. This effect is mediated by the UBA and SH3 domains of UBASH3A, demonstrating a phosphatase-independent function of UBASH3A in T cells (5). We further showed that genetic variants in *UBASH3A* that were associated with risk of type 1 diabetes (T1D) acted by increasing the expression of *UBASH3A* in human primary T cells, leading to reduced IL-2 production upon TCR stimulation (5, 15). Here, we report that

variation in UBASH3A expression modulates cell-surface TCR-CD3 level, suggesting a link between disease-associated genetic variants in *UBASH3A* and TCR-mediated T-cell activation. We show that UBASH3A limits TCR-CD3 expression in resting T cells, and accelerates the downmodulation of cell-surface TCR-CD3 upon TCR engagement via a phosphatase-independent mechanism. In addition, we identify novel interactions of UBASH3A with CBL-B, an E3 ubiquitin ligase that inhibits T-cell activation, and with components of several key cellular processes which regulate TCR-CD3 expression and dynamics. These findings reveal new, phosphatase-independent roles for UBASH3A in TCR signaling in both resting and stimulated human T cells, expanding the mechanisms by which UBASH3A contributes to autoimmunity.

Materials and Methods

Generation of UBASH3A$^{-/-}$ and UBASH3A-overexpressing cell clones

Jurkat (clone E6–1) cells were used to generate UBASH3A$^{-/-}$ clones via CRISPR/Cas9 editing as well as clones expressing V5-tagged UBASH3A, as previously described (5).

Cell lysis and stimulation

Whole-cell lysates were extracted using EBC lysis buffer (50 mM Tris-HCl, pH 7.5, 120 mM NaCl, 0.5% NP-40, and 1 mM EDTA) containing protease and phosphatase inhibitors (cOmplete Mini and PhosSTOP, Roche), as previously described (29). Jurkat cells were stimulated with anti-CD3 and anti-CD28 antibodies, as previously described (5), at 37°C for 3 min, and the resulting cell lysate was subjected to co-immunoprecipitation and immunoblotting. For the quantification of cell-surface CD3ε post stimulation (Fig. 4D), cells were stimulated with 5 μg/mL of plate-bound anti-CD3 antibody (clone OKT3) at 37°C for the indicated periods of time, and then subjected to flow-cytometry analysis.

Site-directed mutagenesis and transfection of HEK293T cells

A cDNA of the full-length human *UBASH3A* was cloned into the Gateway pDONR221 vector (Thermo Fisher Scientific), and the resultant plasmid was used as the template for QuikChange site-directed mutagenesis (Agilent Technologies). The K202R mutation was generated using the primers 5’-gaccttggcccacaggttctacccccacc-3’ and 5’-ggtgggggtagaacctgtgggccaaggtc-3’. The W279A mutation was generated using the primers 5’-gaagccagcgagggcgcggtgattgggatctc-3’ and 5’-gagatcccaatcaccgcgccctcgctggcttc-3’. Next, we performed the LR recombination reaction (Thermo Fisher Scientific) to move the cDNA sequences of wild-type, K202R and W279A *UBASH3A* from the pDONR221 vector to the Gateway pcDNA3.1/nV5-DEST expression vector. The accuracy of all *UBASH3A* inserts was confirmed by Sanger sequencing.

A pBluescriptR plasmid containing the cDNA sequence of full-length human *CBLB* was purchased from Thermo Fisher Scientific, and the *CBLB* cDNA sequence was cloned into the pCMV-Tag2 expression vector (Agilent Technologies) using the restriction enzymes PstI and XhoI (New England BioLabs).

HEK293T cells were transfected with the X-tremeGENE HP DNA Transfection Reagent (Roche), following the manufacturer's protocol.

Co-immunoprecipitation and immunoblotting

For co-immunoprecipitation, 0.5–1 mg of lysate was incubated for 4 h or overnight at 4°C with 1 μg of IgG or the indicated antibody to human CD3ε (rabbit polyclonal, Santa Cruz), CD3ζ (clone 6B10.2, Santa Cruz), PSMC4 (clone H-2, Santa Cruz), UBASH3A (rabbit polyclonal, MilliporeSigma), or V5 (mouse monoclonal, Thermo Fisher Scientific). Next, 20 μL of Protein G Dynabeads (Thermo Fisher Scientific) were added and incubated with the lysate for 1 h at 4°C. The beads were washed four times with EBC lysis buffer (29), and the immunoprecipitates were eluted by heating the beads for 10 min at 70°C in 20 μL of LDS sample buffer (Thermo Fisher Scientific) containing 50 mM DTT.

Whole-cell lysates and the immunoprecipitated samples were resolved on NuPAGE Tris-Acetate or Bolt Bis-Tris Plus gels (Thermo Fisher Scientific). After transfer to PVDF membranes, immunoblotting was performed using the indicated antibody to human CBL-B (clone G-1, Santa Cruz), Dynamin (clone 41/Dynamin, BD Biosciences), HSP70 (rabbit polyclonal, Cell Signaling), γ-tubulin (mouse monoclonal, MilliporeSigma), UBASH3A (rabbit polyclonal; purchased from Proteintech, or custom made by Pacific Immunology using a C-terminal fragment of human UBASH3A (residues 316–623) as the immunogen), V5 (mouse monoclonal, Thermo Fisher Scientific), or ZAP-70 (clone 29/ZAP70 Kinase, BD Biosciences). Chemiluminescence detection was performed using HRP-conjugated secondary antibodies and Western Lightning Plus-ECL Enhanced Chemiluminescence Substrate (PerkinElmer), followed by film exposure or digital imaging with an Amersham Imager 600 (GE Healthcare Life Sciences).

Glutathione S-transferase (GST) pull-down

GST pull-down assays were performed as previously described (5). In brief, whole-cell lysate from unstimulated Jurkat cells was precleared by incubation with Glutathione Sepharose 4B resin (GE Healthcare) for 2 h at 4°C. One milligram of the precleared lysate was incubated for 2 h at 4°C with 20 μL of packed, fresh Glutathione Sepharose 4B resin, and with one of the following at the same molar concentration: 11.6 μg GST-tagged UBA (residues 20–60), 12.6 mg GST-tagged SH3 (residues 241–300), or 22.9 μg GST-tagged PGM (residues 316–623) domain of UBASH3A and 10 μg GST. No-lysate controls contained all the same ingredients as the experimental reactions except for the precleared lysate. After four washes with EBC lysis buffer, eluates were extracted from the resin using LDS sample buffer (Thermo Fisher Scientific) containing 50 mM DTT and analyzed by immunoblotting.

Multiplex fluorescent Western blotting and protein quantification

For CD3ε quantification, blots were blocked with the Odyssey Blocking Buffer in PBS (LI-COR), and then incubated with 1 μg/mL of rabbit anti-CD3ε (Santa Cruz) and 0.4 μg/mL of mouse anti-GAPDH (clone 6C5, Thermo Fisher Scientific). After washing, the blots were incubated with 0.4 μg/mL of Cy3-conjuated goat anti-mouse IgG and 0.4 μg/mL of Cy5-conjugated goat anti-rabbit IgG (GE Healthcare Life Sciences).

For CD3ζ quantification, blots were blocked with 5% nonfat milk in TBS (50 mM Tris-HCl, pH 7.5, and 150 mM NaCl), and then incubated with 1 μg/mL of mouse anti-CD3ζ (clone 6B10.2, Santa Cruz) and 1 μg/mL of rabbit anti-GAPDH (Bio-Rad). After washing, the blots were incubated with 0.2 μg/mL of Alexa Fluor Plus 555-conjugated goat anti-rabbit IgG and 0.2 μg/mL of Alexa Fluor Plus 647-conjugated goat anti-mouse IgG (Thermo Fisher Scientific).

After incubation with the secondary antibodies, the blots were washed, dried, and scanned with a Typhoon 9200 laser scanner (GE Healthcare Life Sciences). Protein bands were quantified using the ImageQuant TL software (GE Healthcare Life Sciences). For each blot (n = 3), the abundances of the target protein (i.e., CD3ε or CD3ζ) in UBASH3A$^{-/-}$ and UBASH3A-overexpressing clones (denoted as X below) relative to that in Jurkat cells were calculated as follows and are shown in Fig. 3: (intensity of target protein in X / intensity of GAPDH in X) / (intensity of target protein in Jurkat / intensity of GAPDH in Jurkat).

Flow-cytometry analysis for cell-surface TCR-CD3 complexes

Jurkat cells and Jurkat-derived UBASH3A$^{-/-}$ and UBASH3A-overexpressing cells were stained with TCR-Vβ8-PE (clone JR2, BioLegend), CD28-PE (clone 37407, R&D), CD3ε-APC (clone HIT3a, BioLegend), CD45-PE (clone 2D1, BioLegend), HLA-B7-PE (clone BB7.1, BioLegend), mouse IgG1-PE (clone MOPC-21, BioLegend), and mouse IgG2a-APC (clone MOPC-173, BioLegend). 7-AAD (BioLegend) was used for dead cell exclusion, and live cells were gated and analyzed. The flow cytometry was conducted on a BD Accuri C6 cytometer, and the data were analyzed using the FlowJo software (Tree Star).

Downmodulation of cell-surface TCR-CD3 upon TCR engagement

To label cell-surface TCR-CD3 complexes, Jurkat cells and Jurkat-derived UBASH3A$^{-/-}$ 2.1F7 and UBASH3A-overexpressing 2F5 cells were incubated with 2.5 μg/mL of APC-conjugated anti-CD3ε (clone HITa3, BioLegend) for 30 min on ice. The cells were washed twice with FACS buffer, and then resuspended in cell culture medium. Next, the cells were incubated at 37°C for the indicated periods of time, ranging from 0 to 60 min; cells that were kept on ice without incubation at 37°C were used for the 0-min time point. After washing the cells twice with cold FACS buffer, the antibodies bound to cell-surface CD3ε were removed by incubating the cells with an acidic buffer (100 mM glycine and 100 mM NaCl, pH 2.5) for 2 min at room temperature, followed by two washes with cold FACS buffer. For the 0-min time point, an equal number of cells were either treated or not treated with the acidic buffer. 7-AAD was used for dead cell exclusion, and the cells were analyzed on a BD Accuri C6 cytometer.

Percentage of internalized CD3ε was calculated as follows: $100 \times [(S_x - S_0)/(T_0 - S_0)]$, where S_x indicates mean APC fluorescence intensity of the cells, at the X-min time point (X = 5, 7.5, 10, 30 or 60), which were treated with the acidic buffer; S_0 mean APC fluorescence intensity of the cells, at the 0-min time point, which were treated with the acidic buffer; T_0 mean APC fluorescence intensity of the cells, at the 0-min time point, which were not treated with the acidic buffer.

Identification of UBASH3A-binding proteins by affinity purification and liquid chromatography-tandem mass spectrometry (LC-MS/MS)

Affinity purification for mass spectrometry

Method 1: Co-immunoprecipitations were performed using a previously described method with modifications (29). In brief, 10 mg of pre-cleared, whole-cell lysate from unstimulated Jurkat cells (experimental sample), or 10 mg of pre-cleared, whole-cell lysate from unstimulated Jurkat-derived UBASH3A$^{-/-}$ cells (negative control), was incubated with 10 μg anti-UBASH3A antibody (MilliporeSigma) overnight at 4°C and subsequently with an additional 50 μL of GammaBind Plus Sepharose beads (GE Healthcare Life Sciences) for 2 h at 4°C. The beads were washed twice with NETN buffer (20 mM Tris-HCl, pH 8.0, 0.6 M NaCl, 0.5% NP-40, and 1 mM EDTA), once with a buffer containing 10 mM Tris-HCl, pH 8.6, 0.1% SDS, 0.05% NP-40, and 0.6 M NaCl, once with NETN buffer, and then twice with PBS. The immunoprecipitates were eluted by heating the beads for 10 min at 70°C in LDS buffer containing 50 mM DTT. The immunoprecipitates were resolved on a NuPAGE 4–12% Bis-Tris gel, followed by silver staining using the SilverQuest kit as per the manufacturer's instruction (Thermo Fisher Scientific). Three regions of the gel where the experimental sample differed from the negative control in staining pattern were excised and subjected to in-gel trypsin digestion. The resulting digested peptides from each excised gel fragment (three for the experimental sample and three for the negative control) were analyzed by LC-MS/MS.

Method 2: Co-immunoprecipitations were conducted similarly as described above for Method 1 with the following modifications. Ten mg of precleared, whole-cell lysate from unstimulated Jurkat-derived UBASH3A-overexpressing cells (experimental sample), or 10 mg of precleared, whole-cell lysate from unstimulated Jurkat cells (negative control), was incubated with 10 μg anti-V5 antibody (Thermo Fisher Scientific) overnight at 4°C and subsequently with an additional 55 μL of GammaBind Plus Sepharose beads for 1 h at 4°C. The beads were washed five times with a buffer containing 50 mM Tris-HCl, pH 7.5, 150 mM NaCl, 1% Triton X-100, and 1 mM EDTA, and then twice with a buffer containing 50 mM Tris-HCl, pH 8.0, and 100 mM NaCl. The immunoprecipitates were eluted by incubating the beads at 37°C for 30 min with 150 μg/mL of V5 peptide (MilliporeSigma) in 50 mM Tris-HCl, pH 8.0, and 100 mM NaCl. V5 peptides in the eluates were removed with Amicon Ultra-0.5 3K devices (MilliporeSigma), following the manufacturer's protocol. The final products from two separate experiments were pooled and then subjected to in-solution trypsin digestion, followed by two rounds of LC-MS/MS.

Method 3: GST pull-down assay was performed, as previously described (5), using whole-cell lysate from Jurkat cells stimulated with anti-CD3 and anti-CD28 antibodies for 3 min. In brief, 6.5 mg of precleared lysate was incubated at 4°C for 2 h with 25 μL Glutathione Sepharose 4B resin (GE Healthcare Life Sciences), and one of the following purified proteins—11.4 μg GST-tagged PGM domain (residues 316–623) of UBASH3A (experimental sample), or 5 μg GST (negative control). The resins were washed four times with a buffer containing 50 mM Tris-HCl, pH 7.5, 150 mM NaCl, 0.5% NP-40, and 1 mM EDTA, and then twice with a buffer containing 50 mM Tris-HCl, pH 8.0, and 150 mM NaCl. For elution, the resins were incubated for 10 min at room temperature with 30 mM reduced

glutathione (MilliporeSigma) in 50 mM Tris-HCl, pH 8.0, and 150 mM NaCl. The eluates were subjected to in-solution trypsin digestion, followed by two rounds of LC-MS/MS.

Trypsin digestion—For in-solution digestion, proteins were solubilized in 50 mM ammonium bicarbonate, pH 8.5, reduced by 10 mM tris(2-carboxyethyl)phosphine at 37°C for 1 h, and alkylated by 20 mM iodoacetamide in the dark for 30 min. Next, the proteins were incubated with trypsin (Promega) (w/w for enzyme : sample = 1 : 100) overnight at 37°C. The digestion was stopped by the addition of 0.1% trifluoroacetic acid (TFA, MilliporeSigma).

For in-gel digestion, a published protocol was used (30), with the modification that the digestion was conducted at 37°C for 15 h in 50 mM ammonium bicarbonate containing 6 μg/mL modified trypsin (Promega). Next, a double extraction was performed, first with 1% formic acid/2% acetonitrile, and then with 80% acetonitrile. The pooled digest was lyophilized and resuspended in 1% formic acid/2% acetonitrile. The ZipTip pipette tips (MilliporeSigma) were used for sample desalting. In brief, after wetting (with 50% acetonitrile) and equilibrating a ZipTip pipette tip (with 0.1% TFA), the peptides were bound to C18 material, washed with 0.1% formic acid, and eluted with 60% acetonitrile and 0.1% formic acid. The samples were dried using a Centrivap SpeedVac vacuum concentrator (Labconco) at 160 mBar.

LC-MS/MS: Mass spectrometry data acquisition was performed on an EASY-nLC 1200 ultraperformance liquid chromatography system (Thermo Fisher Scientific), which was connected to either an Orbitrap Q-Exactive Plus or an Orbitrap Fusion Tribrid instrument (Thermo Fisher Scientific). Trypsin-digested peptides were resuspended in 0.1% formic acid, loaded onto an Acclaim PepMap trapping column (C18, 3 μm, 100 Å, 75 μm i.d. × 2 cm, Thermo Fisher Scientific), and separated on an Acclaim PepMap analytical column (C18, 2 μm, 100 Å, 75 μm i.d. × 25 cm, Thermo Fisher Scientific) using solvent A (0.1% formic acid in water) and solvent B (0.1% formic acid and 99.9% acetonitrile) as the mobile phases.

Peptide and protein identification—The tandem mass spectra were extracted from the Xcalibur.raw files and converted into mgf files using Proteome Discoverer 2.1 (Thermo Fisher Scientific). Charge state deconvolution and deisotoping were not performed. The MS/MS data were searched using the Mascot software (version 2.4.1, Matrix Science) against human protein databases. In Mascot, carbamidomethylation of cysteine was specified as a fixed modification. Gln-to-pyro-Glu of the N-terminus, deamidation of asparagine and glutamine, and oxidation of methionine were specified as variable modifications.

Scaffold version 4.8.6 (Proteome Software) was used to validate MS/MS-based peptide and protein identifications. Peptide identifications were accepted if they could be established at >95.0% probability by the Peptide Prophet algorithm with Scaffold delta-mass correction (31). Protein probabilities were assigned by the Protein Prophet algorithm (32). Protein identifications were accepted if they could be established at >95.0% probability and contained at least one identified peptide. Proteins that contained similar peptides and could

not be differentiated based on MS/MS analysis alone were grouped to satisfy the principles of parsimony. Proteins sharing significant peptide evidence were grouped into clusters.

Proteins identified in both an experimental sample and its corresponding negative control were regarded as nonspecific binding or contamination during sample preparation. The mass spectrometry datasets generated in this study are available in the MassIVE repository (https://massive.ucsd.edu/ProteoSAFe/static/massive.jsp?redirect=auth; MassIVE ID: MSV000082543).

Gene ontology (GO) term enrichment analysis

Functional annotation and enrichment analysis of the GO terms associated with the identified UBASH3A-binding proteins was performed using the Database for Annotation, Visualization and Integrated Discovery (DAVID) program (version 6.8) (33). GOTERM_BP_5 (5th level of biological process ontology) and DAVID's high classification stringency for functional annotation clustering were used in this analysis.

Statistical analysis

Data were analyzed in R (version 3.6.0) using the statistical tests indicated in the figure legends.

Results

Increased UBASH3A expression results in reduced cell-surface expression of TCR-CD3 complexes in unstimulated T cells

The intact TCR-CD3 complex on the surface of αβ T cells exists in 1:1:1:1 stoichiometry for the αβTCR:CD3εγ:CD3εδ:CD3ζζ dimers. To characterize the effect of UBASH3A on TCR-CD3 complex expression, we used flow cytometry to quantify the amounts of cell-surface TCR-CD3 complexes on previously generated Jurkat T-cell clones that were either UBASH3A null as a result of CRISPR/Cas9 editing (Fig. 1A) or expressed V5-tagged UBASH3A (Fig. 1B), both in the absence of TCR activation (5). Increased UBASH3A level led to marked reductions in the amounts of cell-surface CD3ε and TCR-Vβ8 (Fig. 1C, 1E). The knockout of UBASH3A resulted in a modest decrease in the cell-surface level of CD3ε, but not TCR-Vβ8 (Fig. 1D, 1E). Thus, *UBASH3A* deficiency did not considerably alter the amount of cell-surface TCR-CD3 complexes at steady state, which is consistent with previous results in splenocytes from *Ubash3a*$^{-/-}$*Ubash3b*$^{-/-}$ double-knockout mice (1).

UBASH3A interacts with multiple components of the TCR-CD3 complex

It has been previously reported that the SH3 domain of the adaptor protein Nck mediates binding to a proline-rich sequence unique to the cytoplasmic tail of CD3ε, which is not present in other CD3 subunits (34). We tested whether UBASH3A, which also contains an SH3 domain, might similarly bind to CD3ε. Co-immunoprecipitation using lysates from unstimulated Jurkat cells expressing V5-tagged UBASH3A showed that both UBASH3A and its monoubiquitinated form interact with CD3ε (Fig. 2A), but not CD3ζ (data not shown). A GST pull-down assay both confirmed the interaction between UBASH3A and

CD3ε in unstimulated Jurkat cells, and also mapped this interaction primarily to the SH3 domain of UBASH3A (Fig. 2B).

Consistent with previous studies using murine T cells (3, 4), we found that in Jurkat cells stimulated with anti-CD3 plus anti-CD28, UBASH3A co-immunoprecipitated with CD3ζ (Fig. 2C) and ZAP-70 (Fig. 2D). These interactions were not detected in unstimulated Jurkat cells (Fig. 2C, 2D). These findings indicate that UBASH3A not only binds to CD3ε in resting T cells, but also plays a role in proximal TCR signaling upon TCR stimulation.

UBASH3A regulates the total amounts of CD3ε and CD3ζ

The steady-state level of cell-surface TCR-CD3 complexes results from a complex equilibrium between the synthesis and secretion of new TCR and CD3 polypeptides and their internalization, followed by recycling or degradation (35–37). To determine whether the reduction in cell-surface TCR-CD3 level associated with UBASH3A expression results from changes in the total amounts of CD3 chains, we quantified CD3ε and CD3ζ by multiplex fluorescent immunoblotting in two UBASH3A-overexpressing clones and two UBASH3A$^{-/-}$ clones, as well as in the parental Jurkat cells. UBASH3A deficiency had no significant effect on the total amount of CD3ε or CD3ζ (Fig. 3A, 3B). In contrast, increased UBASH3A expression resulted in less total CD3ζ in both the 5E4 and the 2F5 clones (Fig. 3B). A significant effect of UBASH3A expression on the total amount of CD3ε was observed only in the 2F5 clone (Fig. 3A), which expresses more exogenous UBASH3A than the 5E4 clone (Fig. 1B) (5). These findings suggest that UBASH3A may promote the degradation of CD3 chains. The differential dose effect of UBASH3A expression on CD3ε and CD3ζ likely reflects the fact that CD3ζ is synthesized at approximately one-tenth the level of the other CD3 chains (35), and that in resting T cells, CD3ζ may be degraded at a higher rate than the other CD3 subunits (36).

UBASH3A facilitates the downmodulation of cell-surface TCR-CD3 complexes upon TCR engagement

TCR-CD3 complexes are continuously endocytosed and recycled in resting T cells (36–38). TCR ligation triggers rapid downmodulation of cell-surface TCR-CD3, as a result of enhanced internalization of TCR-CD3 complexes and their degradation in lysosomes and proteasomes, and decreased recycling of internalized TCR-CD3 back to the plasma membrane (36–38). One essential component for TCR-CD3 endocytosis is the protein dynamin (39), which has been reported to interact with UBASH3A when both proteins are ectopically overexpressed in HeLa cells (20). Using lysates from unstimulated Jurkat cells expressing V5-tagged UBASH3A, we were able to co-immunoprecipitate dynamin and UBASH3A indicating that this interaction also occurs in T cells where UBASH3A is normally expressed (Fig. 4A).

Based on the observed interaction between UBASH3A and dynamin, we evaluated the possibility that UBASH3A regulates the turnover of cell-surface TCR-CD3 complexes upon TCR engagement. Briefly, Jurkat, UBASH3A$^{-/-}$ 2.1F7, and UBASH3A-overexpressing 2F5 cells were labeled with APC-conjugated anti-CD3ε antibodies, incubated at 37°C for various periods of time, and stripped. The amount of internalized antibodies was quantified

by flow cytometry. Compared to the parental Jurkat cells, increased expression of UBASH3A led to accelerated internalization of cell-surface CD3ε at 5 min (Fig. 4B, 4C). In contrast, UBASH3A deficiency resulted in reductions in internalized cell-surface CD3ε at 30 min and 60 min (Fig. 4B, 4C). In addition, increased UBASH3A expression led to diminished amounts of cell-surface CD3ε at 0 and 5 min after anti-CD3 stimulation (Fig. 4D). Together, these results suggest that UBASH3A may facilitate the endocytosis of cell-surface TCR-CD3 complexes, and/or inhibit their recycling back to the plasma membrane.

UBASH3A interacts with multiple proteins involved in receptor synthesis, endocytosis and endocytic recycling

Given the complexity of the cellular pathways involved in the synthesis, trafficking and turnover of TCR-CD3 complexes, we sought to gain insight into the potential role(s) of UBASH3A in these processes through the identification of UBASH3A-binding partners in T cells. We performed co-immunoprecipitations, using lysates from unstimulated Jurkat cells or Jurkat cells expressing V5-tagged UBASH3A, and identified peptides by LC-MS/MS. In addition, we conducted a GST pull-down assay using lysates from stimulated Jurkat cells and the GST-tagged PGM domain (residues 316–623) of UBASH3A, and the products were analyzed by LC-MS/MS.

In total, our proteomic experiments identified over 60 proteins that interact with UBASH3A, many of which were not included in the BioGRID interaction database (40). An analysis of GO terms associated with these proteins revealed significant enrichment for pathways involved in immune response signaling, activation and regulation, as well as pathways involved in protein targeting and turnover (Fig. 5 and Supplemental Table I). Consistent with our prior results linking UBASH3A with TCR-CD3 components, we identified a number of novel interacting partners for UBASH3A with established roles in the synthesis, turnover or recycling of TCR-CD3 (Supplemental Table II). These included proteins of the endoplasmic-reticulum-associated protein degradation (ERAD) pathway, a key component of the protein quality control machinery in the ER. Both TCRα and CD3δ are known ERAD substrates (41, 42). UBASH3A also bound to two subunits of the 26S proteasome, and a negative regulator of the proteasome; several molecular chaperones central to the selection of ERAD substrates, such as members of the heat shock 70 kDa (HSP70) and 90 kDa families; and VCP, a component of the Cdc48 complex, which pulls polyubiquitinated substrates from the ER membrane and delivers them to the proteasome for degradation (Supplemental Table II) (43, 44). We verified, in separate co-immunoprecipitation experiments, the interaction of UBASH3A with HSP70 (Fig. 6A), and with the 26S proteasome regulatory subunit 6B (PSMC4) in unstimulated Jurkat cells (Fig. 6B).

UBASH3A also interacts with components of the endocytic recycling pathway (ARF1/3 and RAB11A/11B) (45, 46); HIP1, a protein involved in clathrin-mediated endocytosis and trafficking (47); and cytoskeletal proteins, such as β-actin, α-tubulin and β-tubulin, which is consistent with a previous report (21) (Supplemental Table II).

Taken together, our functional data, supported by our proteomic results and enrichment analysis, suggest that UBASH3A plays a significant role in the synthesis and turnover of

TCR-CD3 in the cytoplasm, likely via ERAD, as well as in the dynamics and equilibrium of cell-surface TCR-CD3 via endocytosis and recycling.

UBASH3A binds to CBL-B via its SH3 domain

CBL and CBL-B are two highly homologous RING-type E3 ubiquitin ligases, and they have been shown to negatively regulate thymocyte development and peripheral T-cell activation, respectively (48–54). CBL has been previously reported to interact with UBASH3A (21, 22) and was readily detected in our proteomic analysis of UBASH3A co-immunoprecipitates (Supplemental Table II). The distinction between CBL and CBL-B in terms of substrate specificity and the role of CBL-B in regulating the CD28 dependence of T-cell activation (51, 52) prompted us to examine whether UBASH3A also interacts with CBL-B in T cells. We found that in unstimulated Jurkat cells, UBASH3A and CBL-B co-immunoprecipitated (Fig. 7A), and this interaction is mediated by the SH3 domain of UBASH3A (Supplemental Fig. 1).

To further verify the role of the SH3 domain in the interaction between UBASH3A and CBL-B, we generated the K202R and W279A UBASH3A mutants, where the major ubiquitination site or the function of the SH3 domain was obliterated, respectively (19, 21). HEK293T cells were co-transfected with a construct encoding FLAG-tagged CBL-B and one of the following V5-tagged UBASH3A constructs—wild-type, K202R, or W279A. As expected, the K202R mutation led to a marked reduction in the amount of monoubiquitinated UBASH3A, whereas the W279A mutation did not affect monoubiquitination of UBASH3A (Fig. 7B). Neither the K202R nor the W279A mutation altered CBL-B levels (Fig. 7B). Lysates from these co-transfected HEK293T cells were subjected to co-immunoprecipitation and immunoblotting analysis. We confirmed that the SH3 domain of UBASH3A mediates its binding to CBL-B, as demonstrated by the disruptive effect of the W279A mutation (Fig. 7C); and that this interaction does not involve the K202 major ubiquitination site (Fig. 7C).

UBASH3A does not affect cell-surface CD28 level in unstimulated T cells

CD28 is a crucial co-stimulatory receptor on T cells. CD28-triggered signaling, in addition to TCR signaling, is required for optimal T-cell activation. Given our finding that UBASH3A interacts with CBL-B, we examined whether UBASH3A influences the amount of cell-surface CD28 in unstimulated T cells, analogous to our observations for TCR-CD3. Flow-cytometry analysis showed that without TCR stimulation, modulation of UBASH3A levels in Jurkat cells did not affect the amount of cell-surface CD28 (Fig. 8A). No statistically significant changes in the MFI of cell-surface CD28 were observed in UBASH3A$^{-/-}$ or UBASH3A-overexpressing cells, compared to that in the parental Jurkat cells (Fig. 8A). Furthermore, modulation of UBASH3A expression did not affect the cell-surface expression of the membrane proteins CD45 and HLA-B7 (Fig. 8B, 8C). These data show that in unstimulated T cells, UBASH3A regulates cell-surface TCR-CD3 without affecting cell-surface CD28.

Discussion

Our study springs from the initial observation that modulation of UBASH3A levels in unstimulated Jurkat cells results in significant variation in the level of TCR-CD3 complexes on the plasma membrane. This observation is important in that TCR-CD3 cell-surface expression is tightly regulated during T-cell development in the thymus, as well as in mature T cells in both resting and stimulated conditions. In addition, we have previously shown that T1D-associated alleles at genetic variants within the *UBASH3A* gene confer disease risk by increasing the expression level of *UBASH3A* (5, 15). Our mechanistic studies, reported here, show that UBASH3A has multiple, previously unrecognized impacts on TCR-CD3 synthesis, equilibrium and dynamics—both in resting T cells and in cells responding to TCR engagement—that are quantitatively dependent on UBASH3A expression levels.

Our characterization of Jurkat T-cell clones engineered to be either UBASH3A null or express graded amounts of epitope-tagged UBASH3A suggests the following model for the role of UBASH3A in modulating TCR-CD3 levels. In unstimulated T cells, UBASH3A enhances the degradation of CD3 subunits in the ER, most likely via the ERAD machinery, as it interacts with multiple ERAD components. Increased expression level of UBASH3A in unstimulated T cells leads to a decrease in the level of cell-surface TCR-CD3, as well as in the total amounts of CD3ε and CD3ζ, the latter of which is affected by UBASH3A in a dose-dependent manner, and is rate limiting for the assembly of TCR-CD3 complexes before they are transported to the plasma membrane (35, 36). Upon TCR engagement, UBASH3A further promotes the downmodulation of cell-surface TCR-CD3. This effect, together with the aforementioned effect of UBASH3A on TCR-CD3 levels in resting state, results in dampened proximal TCR-CD3 signaling and consequently less IL-2 production. The protein-protein interactions we detected by mass spectrometry, particularly by Method 3 (Supplemental Table II) which utilized stimulated Jurkat cells, include proteins involved in receptor endocytosis, recycling, and proteasome degradation, suggesting that the role of UBASH3A in TCR-CD3 receptor downmodulation may be complex. We show that UBASH3A also interacts with phosphorylated CD3ζ and ZAP-70 upon TCR stimulation, but these interactions may be indirect, occurring as a consequence of the binding of CBL to these phosphorylated molecules upon stimulation (55, 56).

Our proteomic studies have significantly increased the number of reported protein-protein interactions that involve UBASH3A, and our GO term enrichment analysis provides statistical evidence for the previously unrecognized role of UBASH3A in protein targeting, localization and turnover. Many of the 26 human UBASH3A-interacting partners in the BioGRID database are either ubiquitin-related molecules or tyrosine phosphorylated signaling molecules and their associated tyrosine kinases and adaptor proteins. In contrast, in both resting and stimulated Jurkat cells, we identified, by both co-immunoprecipitation and GST pull-down, peptides from multiple components of the ERAD pathway in association with UBASH3A. ERAD recognizes misfolded or incompletely processed polypeptides, ejects them from the ER, and returns them to the cytoplasm, where these polypeptides are ubiquitinated and then degraded by the 26S proteasome (43, 44). The reductions in cellular levels of CD3ε and CD3ζ observed when UBASH3A expression is

increased may reflect increased activity of ERAD—further studies will be required to determine how UBASH3A impacts this pathway.

Given the observed effects of UBASH3A on TCR-CD3 complexes, we were motivated to search for interaction between UBASH3A and CD28, a critical co-stimulatory receptor that acts cooperatively with TCR-CD3 in T-cell activation. While we did not detect any interaction between CD28 and UBASH3A by co-immunoprecipitation (Supplemental Fig. 2), we did detect interaction between UBASH3A and CBL-B, which regulates the CD28 dependence of T-cell activation. Previously, we reported that UBASH3A inhibits NF-κB signaling in human T cells, and that T1D-risk alleles in *UBASH3A* lead to elevated *UBASH3A* expression and hence diminished *IL2* expression (5). Notably, CBL-B also suppresses NF-κB signaling (57) and IL-2 production in T cells (51, 52). Furthermore, a mutation in *Cblb* is, together with a permissive MHC allele, responsible for autoimmune diabetes in the Komeda diabetes-prone rat model (58). A recent genome-wide CRISPR screen in human primary $CD8^+$ T cells identified both UBASH3A and CBL-B as key negative regulators of T-cell proliferation upon TCR stimulation (6). These previous findings, together with our newly observed interaction between UBASH3A and CBL-B, raise the possibility that UBASH3A and CBL-B may have synergistic effects on T-cell activation and function, and on the development of T1D, as genetic variants in both genes have been identified to be associated with the disease (7–14, 58).

In summary, in the current study, we show that variation in the expression level of UBASH3A in human T cells modulates both the cell-surface level of TCR-CD3 complexes as well as the total cellular levels of selected CD3 components. Novel interactions of UBASH3A with multiple proteins involved in receptor endocytosis, recycling and degradation are identified, consistent with the observed effects of UBASH3A on TCR-CD3 turnover. In addition, UBASH3A interacts with another independent negative regulator of NF-κB signaling, CBL-B. Each of these observed effects of altered UBASH3A amount on TCR-CD3 expression, inhibition of NF-κB signaling (5), and interaction with CBL-B are complementary and consistent with a model in which UBASH3A acts as a negative regulator of T-cell activation via both TCR proximal and distal signaling effects, which, together, result in reduced IL-2 secretion.

Supplementary Material

Refer to Web version on PubMed Central for supplementary material.

Acknowledgments

The authors thank the Proteomics & Mass Spectrometry Core of the Interdisciplinary Center for Biotechnology Research (ICBR) at the University of Florida for acquiring the mass spectrometry data and performing database searching.

This work was supported by National Institute of Diabetes and Digestive and Kidney Diseases grants DK106718, DK046635, and DK085678 (to P.C.) and by an Advanced Postdoctoral Fellowship award (3-APF-2016–177-A-N) from Juvenile Diabetes Research Foundation (to Y.G.).

Glossary

ERAD	endoplasmic-reticulum-associated protein degradation
GO	gene ontology
GST	glutathione S-transferase
HSP70	heat shock 70kDa proteins
LC-MS/MS	liquid chromatography-tandem mass spectrometry
MFI	median fluorescence intensity
PGM	phosphoglycerate mutase-like
PSMC4	26S proteasome regulatory subunit 6B
SH3	SRC homology 3
T1D	type 1 diabetes
TCR	T-cell receptor
TFA	trifluoroacetic acid
UBA	ubiquitin-associated
UBASH3A	Ubiquitin-associated and SH3 containing A

References

1. Carpino N, Turner S, Mekala D, Takahashi Y, Zang H, Geiger TL, Doherty P, and Ihle JN. 2004 Regulation of ZAP-70 activation and TCR signaling by two related proteins, Sts-1 and Sts-2. Immunity 20: 37–46. [PubMed: 14738763]
2. San Luis B, Sondgeroth B, Nassar N, and Carpino N. 2011 Sts-2 is a phosphatase that negatively regulates zeta-associated protein (ZAP)-70 and T cell receptor signaling pathways. J. Biol. Chem 286: 15943–15954. [PubMed: 21393235]
3. Yang M, Chen T, Li X, Yu Z, Tang S, Wang C, Gu Y, Liu Y, Xu S, Li W, Zhang X, Wang J, and Cao X. 2015 K33-linked polyubiquitination of Zap70 by Nrdp1 controls $CD8^+$ T cell activation. Nat. Immunol 16: 1253–1262. [PubMed: 26390156]
4. Hu H, Wang H, Xiao Y, Jin J, Chang J-H, Zou Q, Xie X, Cheng X, and Sun S-C. 2016 Otud7b facilitates T cell activation and inflammatory responses by regulating Zap70 ubiquitination. J. Exp. Med 213: 399–414. [PubMed: 26903241]
5. Ge Y, Paisie TK, Newman JRB, McIntyre LM, and Concannon P. 2017 UBASH3A mediates risk for type 1 diabetes through inhibition of T-cell receptor-induced NF-κB signaling. Diabetes 66: 2033–2043. [PubMed: 28607106]
6. Shifrut E, Carnevale J, Tobin V, Roth TL, Woo JM, Bui CT, Li PJ, Diolaiti ME, Ashworth A, and Marson A. 2018 Genome-wide CRISPR Screens in Primary Human T Cells Reveal Key Regulators of Immune Function. Cell 175: 1958–1971.e15. [PubMed: 30449619]
7. Concannon P, Onengut-Gumuscu S, Todd JA, Smyth DJ, Pociot F, Bergholdt R, Akolkar B, Erlich HA, Hilner JE, Julier C, Morahan G, Nerup J, Nierras CR, Chen W-M, Rich SS, and the T. 1 D. G. Consortium. 2008 A human type 1 diabetes susceptibility locus maps to chromosome 21q22.3. Diabetes 57: 2858–2861. [PubMed: 18647951]

8. Smyth DJ, Plagnol V, Walker NM, Cooper JD, Downes K, Yang JHM, Howson JMM, Stevens H, McManus R, Wijmenga C, Heap GA, Dubois PC, Clayton DG, Hunt KA, van Heel DA, and Todd JA. 2008 Shared and distinct genetic variants in type 1 diabetes and celiac disease. N. Engl. J. Med 359: 2767–2777. [PubMed: 19073967]

9. Barrett JC, Clayton DG, Concannon P, Akolkar B, Cooper JD, Erlich HA, Julier C, Morahan G, Nerup J, Nierras C, Plagnol V, Pociot F, Schuilenburg H, Smyth DJ, Stevens H, Todd JA, Walker NM, and Rich SS. 2009 Genome-wide association study and meta-analysis find that over 40 loci affect risk of type 1 diabetes. Nat. Genet 41: 703–707. [PubMed: 19430480]

10. Grant SFA, Qu H-Q, Bradfield JP, Marchand L, Kim CE, Glessner JT, Grabs R, Taback SP, Frackelton EC, Eckert AW, Annaiah K, Lawson ML, Otieno FG, Santa E, Shaner JL, Smith RM, Skraban R, Imielinski M, Chiavacci RM, Grundmeier RW, Stanley CA, Kirsch SE, Waggott D, Paterson AD, Monos DS, the D. R. Group, Polychronakos C, and Hakonarson H. 2009 Follow-up analysis of genome-wide association data identifies novel loci for type 1 diabetes. Diabetes 58: 290–295. [PubMed: 18840781]

11. Plagnol V, Howson JMM, Smyth DJ, Walker N, Hafler JP, Wallace C, Stevens H, Jackson L, Simmonds MJ, Type 1 Diabetes Genetics Consortium, Bingley PJ, Gough SC, and Todd JA. 2011 Genome-wide association analysis of autoantibody positivity in type 1 diabetes cases. PLoS Genet 7: e1002216. [PubMed: 21829393]

12. Johnson K, Wong R, Barriga KJ, Klingensmith G, Ziegler A-G, Rewers MJ, and Steck AK. 2012 rs11203203 is associated with type 1 diabetes risk in population pre-screened for high-risk HLA-DR,DQ genotypes. Pediatr. Diabetes 13: 611–615. [PubMed: 22776074]

13. Frederiksen BN, Steck AK, Kroehl M, Lamb MM, Wong R, Rewers M, and Norris JM. 2013 Evidence of stage- and age-related heterogeneity of non-HLA SNPs and risk of islet autoimmunity and type 1 diabetes: the diabetes autoimmunity study in the young. Clin. Dev. Immunol 2013: 417657. [PubMed: 24367383]

14. Onengut-Gumuscu S, Chen W-M, Burren O, Cooper NJ, Quinlan AR, Mychaleckyj JC, Farber E, Bonnie JK, Szpak M, Schofield E, Achuthan P, Guo H, Fortune MD, Stevens H, Walker NM, Ward LD, Kundaje A, Kellis M, Daly MJ, Barrett JC, Cooper JD, Deloukas P, Type 1 Diabetes Genetics Consortium, Todd JA, Wallace C, Concannon P, and Rich SS. 2015 Fine mapping of type 1 diabetes susceptibility loci and evidence for colocalization of causal variants with lymphoid gene enhancers. Nat. Genet 47: 381–386. [PubMed: 25751624]

15. Ge Y, and Concannon P. 2018 Molecular-genetic characterization of common, noncoding *UBASH3A* variants associated with type 1 diabetes. Eur. J. Hum. Genet 26: 1060–1064. [PubMed: 29491471]

16. Jin Y, Birlea SA, Fain PR, Gowan K, Riccardi SL, Holland PJ, Mailloux CM, Sufit AJD, Hutton SM, Amadi-Myers A, Bennett DC, Wallace MR, McCormack WT, Kemp EH, Gawkrodger DJ, Weetman AP, Picardo M, Leone G, Taïeb A, Jouary T, Ezzedine K, van Geel N, Lambert J, Overbeck A, and Spritz RA. 2010 Variant of *TYR* and autoimmunity susceptibility loci in generalized vitiligo. N. Engl. J. Med 362: 1686–1697. [PubMed: 20410501]

17. Zhernakova A, Stahl EA, Trynka G, Raychaudhuri S, Festen EA, Franke L, Westra H-J, Fehrmann RSN, Kurreeman FAS, Thomson B, Gupta N, Romanos J, McManus R, Ryan AW, Turner G, Brouwer E, Posthumus MD, Remmers EF, Tucci F, Toes R, Grandone E, Mazzilli MC, Rybak A, Cukrowska B, Coenen MJH, Radstake TRDJ, van Riel PLCM, Li Y, de Bakker PIW, Gregersen PK, Worthington J, Siminovitch KA, Klareskog L, Huizinga TWJ, Wijmenga C, and Plenge RM. 2011 Meta-analysis of genome-wide association studies in celiac disease and rheumatoid arthritis identifies fourteen non-HLA shared loci. PLoS Genet 7: e1002004. [PubMed: 21383967]

18. Diaz-Gallo L-M, Sánchez E, Ortego-Centeno N, Sabio JM, García-Hernández FJ, de Ramón E, González-Gay MA, Witte T, Anders H-J, González-Escribano MF, and Martin J. 2013 Evidence of new risk genetic factor to systemic lupus erythematosus: the UBASH3A gene. PLoS One 8: e60646. [PubMed: 23565265]

19. Hoeller D, Crosetto N, Blagoev B, Raiborg C, Tikkanen R, Wagner S, Kowanetz K, Breitling R, Mann M, Stenmark H, and Dikic I. 2006 Regulation of ubiquitin-binding proteins by monoubiquitination. Nat. Cell Biol 8: 163–169. [PubMed: 16429130]

20. Bertelsen V, Breen K, Sandvig K, Stang E, and Madshus IH. 2007 The Cbl-interacting protein TULA inhibits dynamin-dependent endocytosis. Exp. Cell Res 313: 1696–1709. [PubMed: 17382318]
21. Feshchenko EA, Smirnova EV, Swaminathan G, Teckchandani AM, Agrawal R, Band H, Zhang X, Annan RS, Carr SA, and Tsygankov AY. 2004 TULA: an SH3- and UBA-containing protein that binds to c-Cbl and ubiquitin. Oncogene 23: 4690–4706. [PubMed: 15107835]
22. Kowanetz K, Crosetto N, Haglund K, Schmidt MHH, Heldin C-H, and Dikic I. 2004 Suppressors of T-cell receptor signaling Sts-1 and Sts-2 bind to Cbl and inhibit endocytosis of receptor tyrosine kinases. J. Biol. Chem 279: 32786–32795. [PubMed: 15159412]
23. Wattenhofer M, Shibuya K, Kudoh J, Lyle R, Michaud J, Rossier C, Kawasaki K, Asakawa S, Minoshima S, Berry A, Bonne-Tamir B, Shimizu N, Antonarakis S, and Scott H. 2001 Isolation and characterization of the *UBASH3A* gene on 21q22.3 encoding a potential nuclear protein with a novel combination of domains. Hum. Genet 108: 140–147. [PubMed: 11281453]
24. Chen Y, Jakoncic J, Carpino N, and Nassar N. 2009 Structural and functional characterization of the 2H-phosphatase domain of Sts-2 reveals an acid-dependent phosphatase activity. Biochemistry 48: 1681–1690. [PubMed: 19196006]
25. Mikhailik A, Ford B, Keller J, Chen Y, Nassar N, and Carpino N. 2007 A phosphatase activity of Sts-1 contributes to the suppression of TCR signaling. Mol. Cell 27: 486–497. [PubMed: 17679096]
26. Agrawal R, Carpino N, and Tsygankov A. 2008 TULA proteins regulate activity of the protein tyrosine kinase Syk. J. Cell. Biochem 104: 953–964. [PubMed: 18189269]
27. Chen X, Ren L, Kim S, Carpino N, Daniel JL, Kunapuli SP, Tsygankov AY, and Pei D. 2010 Determination of the substrate specificity of protein-tyrosine phosphatase TULA-2 and identification of Syk as a TULA-2 substrate. J. Biol. Chem 285: 31268–31276. [PubMed: 20670933]
28. Thomas DH, Getz TM, Newman TN, Dangelmaier CA, Carpino N, Kunapuli SP, Tsygankov AY, and Daniel JL. 2010 A novel histidine tyrosine phosphatase, TULA-2, associates with Syk and negatively regulates GPVI signaling in platelets. Blood 116: 2570–2578. [PubMed: 20585042]
29. Ge Y, Onengut-Gumuscu S, Quinlan AR, Mackey AJ, Wright JA, Buckner JH, Habib T, Rich SS, and Concannon P. 2016 Targeted deep sequencing in multiple-affected sibships of European ancestry identifies rare deleterious variants in *PTPN22* that confer risk for type 1 diabetes. Diabetes 65: 794–802. [PubMed: 26631741]
30. Rosenfeld J, Capdevielle J, Guillemot JC, and Ferrara P. 1992 In-gel digestion of proteins for internal sequence analysis after one- or two-dimensional gel electrophoresis. Anal. Biochem 203: 173–179. [PubMed: 1524213]
31. Keller A, Nesvizhskii AI, Kolker E, and Aebersold R. 2002 Empirical statistical model to estimate the accuracy of peptide identifications made by MS/MS and database search. Anal. Chem 74: 5383–5392. [PubMed: 12403597]
32. Nesvizhskii AI, Keller A, Kolker E, and Aebersold R. 2003 A statistical model for identifying proteins by tandem mass spectrometry. Anal. Chem 75: 4646–4658. [PubMed: 14632076]
33. Huang DW, Sherman BT, and Lempicki RA. 2009 Bioinformatics enrichment tools: paths toward the comprehensive functional analysis of large gene lists. Nucleic Acids Res 37: 1–13. [PubMed: 19033363]
34. Gil D, Schamel WWA, Montoya M, Sánchez-Madrid F, and Alarcón B. 2002 Recruitment of Nck by CD3ε reveals a ligand-induced conformational change essential for T cell receptor signaling and synapse formation. Cell 109: 901–912. [PubMed: 12110186]
35. Klausner RD, Lippincott-Schwartz J, and Bonifacino JS. 1990 The T cell antigen receptor: insights into organelle biology. Annu. Rev. Cell Biol 6: 403–431. [PubMed: 2275818]
36. Alcover A, and Alarcón B. 2000 Internalization and intracellular fate of TCR-CD3 complexes. Crit. Rev. Immunol 20: 325–346. [PubMed: 11100805]
37. Geisler C 2004 TCR trafficking in resting and stimulated T cells. Crit. Rev. Immunol 24: 67–86. [PubMed: 14995914]
38. Liu H, Rhodes M, Wiest DL, and Vignali DAA. 2000 On the dynamics of TCR:CD3 complex cell surface expression and downmodulation. Immunity 13: 665–675. [PubMed: 11114379]

39. Compeer EB, Kraus F, Ecker M, Redpath G, Amiezer M, Rother N, Nicovich PR, Kapoor-Kaushik N, Deng Q, Samson GPB, Yang Z, Lou J, Carnell M, Vartoukian H, Gaus K, and Rossy J. 2018 A mobile endocytic network connects clathrin-independent receptor endocytosis to recycling and promotes T cell activation. Nat. Commun 9: 1597. [PubMed: 29686427]
40. Stark C, Breitkreutz B-J, Reguly T, Boucher L, Breitkreutz A, and Tyers M. 2006 BioGRID: a general repository for interaction datasets. Nucleic Acids Res 34: D535–539. [PubMed: 16381927]
41. Yang M, Omura S, Bonifacino JS, and Weissman AM. 1998 Novel aspects of degradation of T cell receptor subunits from the endoplasmic reticulum (ER) in T cells: importance of oligosaccharide processing, ubiquitination, and proteasome-dependent removal from ER membranes. J. Exp. Med 187: 835–846. [PubMed: 9500786]
42. Tiwari S, and Weissman AM. 2001 Endoplasmic reticulum (ER)-associated degradation of T cell receptor subunits. Involvement of ER-associated ubiquitin-conjugating enzymes (E2s). J. Biol. Chem 276: 16193–16200. [PubMed: 11278356]
43. Stolz A, and Wolf DH. 2010 Endoplasmic reticulum associated protein degradation: a chaperone assisted journey to hell. Biochim. Biophys. Acta 1803: 694–705. [PubMed: 20219571]
44. Brodsky JL 2012 Cleaning up: ER-associated degradation to the rescue. Cell 151: 1163–1167. [PubMed: 23217703]
45. Kondo Y, Hanai A, Nakai W, Katoh Y, Nakayama K, and Shin H-W. 2012 ARF1 and ARF3 are required for the integrity of recycling endosomes and the recycling pathway. Cell Struct. Funct 37: 141–154. [PubMed: 22971977]
46. Takahashi S, Kubo K, Waguri S, Yabashi A, Shin H-W, Katoh Y, and Nakayama K. 2012 Rab11 regulates exocytosis of recycling vesicles at the plasma membrane. J Cell Sci 125: 4049–4057. [PubMed: 22685325]
47. Hyun TS, and Ross TS. 2004 HIP1: trafficking roles and regulation of tumorigenesis. Trends Mol. Med 10: 194–199. [PubMed: 15059611]
48. Murphy MA, Schnall RG, Venter DJ, Barnett L, Bertoncello I, Thien CB, Langdon WY, and Bowtell DD. 1998 Tissue hyperplasia and enhanced T-cell signalling via ZAP-70 in c-Cbl-deficient mice. Mol. Cell. Biol 18: 4872–4882. [PubMed: 9671496]
49. Naramura M, Kole HK, Hu RJ, and Gu H. 1998 Altered thymic positive selection and intracellular signals in Cbl-deficient mice. Proc. Natl. Acad. Sci. U. S. A 95: 15547–15552. [PubMed: 9861006]
50. Thien CB, Bowtell DD, and Langdon WY. 1999 Perturbed regulation of ZAP-70 and sustained tyrosine phosphorylation of LAT and SLP-76 in c-Cbl-deficient thymocytes. J. Immunol 162: 7133–7139. [PubMed: 10358158]
51. Bachmaier K, Krawczyk C, Kozieradzki I, Kong YY, Sasaki T, Oliveira-dos-Santos A, Mariathasan S, Bouchard D, Wakeham A, Itie A, Le J, Ohashi PS, Sarosi I, Nishina H, Lipkowitz S, and Penninger JM. 2000 Negative regulation of lymphocyte activation and autoimmunity by the molecular adaptor Cbl-b. Nature 403: 211–216. [PubMed: 10646608]
52. Chiang YJ, Kole HK, Brown K, Naramura M, Fukuhara S, Hu R-J, Jang IK, Gutkind JS, Shevach E, and Gu H. 2000 Cbl-b regulates the CD28 dependence of T-cell activation. Nature 403: 216–220. [PubMed: 10646609]
53. Liu Y-C, and Gu H. 2002 Cbl and Cbl-b in T-cell regulation. Trends Immunol 23: 140–143. [PubMed: 11864842]
54. Lutz-Nicoladoni C, Wolf D, and Sopper S. 2015 Modulation of immune cell functions by the E3 ligase Cbl-b. Front. Oncol 5: 58. [PubMed: 25815272]
55. Lupher ML, Reedquist KA, Miyake S, Langdon WY, and Band H. 1996 A novel phosphotyrosine-binding domain in the N-terminal transforming region of Cbl interacts directly and selectively with ZAP-70 in T cells. J. Biol. Chem 271: 24063–24068. [PubMed: 8798643]
56. Wang HY, Altman Y, Fang D, Elly C, Dai Y, Shao Y, and Liu YC. 2001 Cbl promotes ubiquitination of the T cell receptor ζ through an adaptor function of Zap-70. J. Biol. Chem 276: 26004–26011. [PubMed: 11353765]
57. Qiao G, Li Z, Molinero L, Alegre M-L, Ying H, Sun Z, Penninger JM, and Zhang J. 2008 T-cell receptor-induced NF-κB activation is negatively regulated by E3 ubiquitin ligase Cbl-b. Mol. Cell. Biol 28: 2470–2480. [PubMed: 18227156]

58. Yokoi N, Komeda K, Wang H-Y, Yano H, Kitada K, Saitoh Y, Seino Y, Yasuda K, Serikawa T, and Seino S. 2002 *Cblb* is a major susceptibility gene for rat type 1 diabetes mellitus. Nat. Genet 31: 391–394. [PubMed: 12118252]

Key points

UBASH3A interacts with the TCR-CD3 complex and regulates its turnover.

UBASH3A facilitates the downmodulation of cell-surface TCR-CD3 upon TCR engagement.

UBASH3A binds to CBL-B, another T1D-associated protein that inhibits T-cell function.

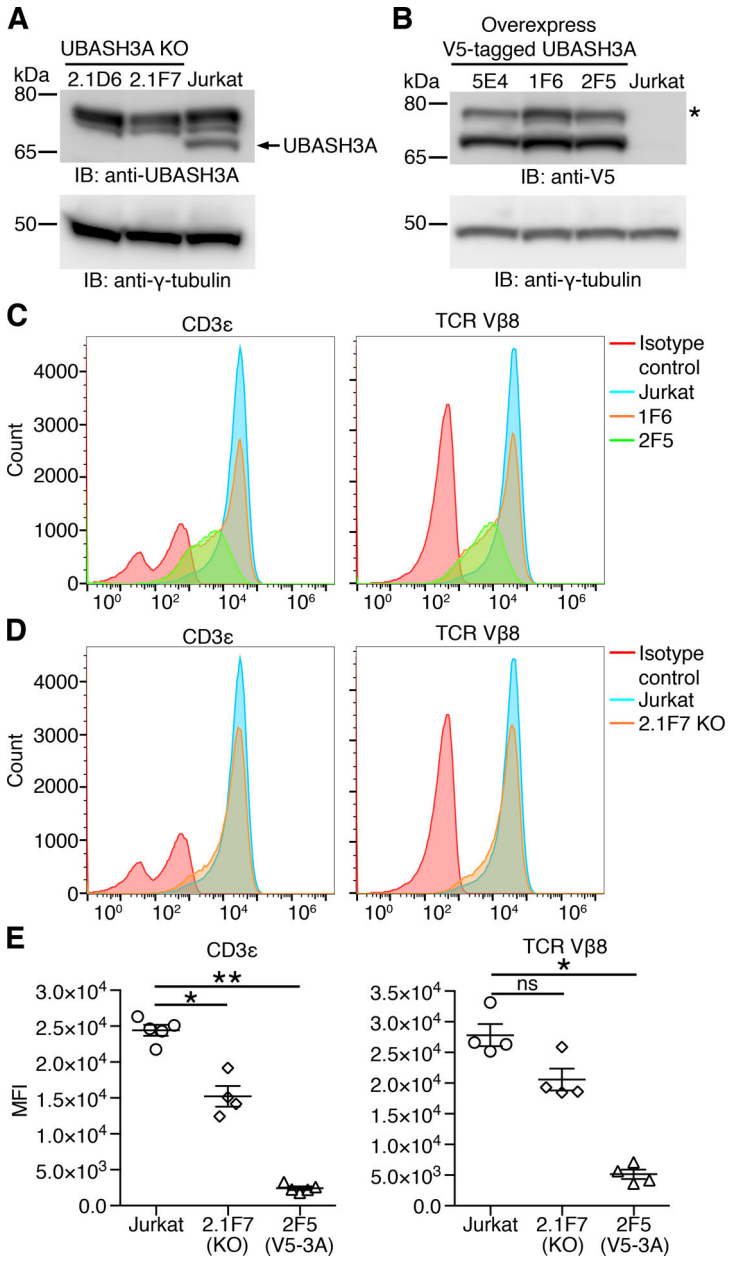

FIGURE 1.

UBASH3A modulates the amount of cell-surface TCR-CD3 complexes in unstimulated T cells. (**A**) Lysates from unstimulated Jurkat cells and from two Jurkat-derived UBASH3A$^{-/-}$ clones (2.1D6 and 2.1F7) were subjected to immunoblotting with anti-UBASH3A and subsequently with anti-γ-tubulin after stripping. (**B**) Lysates from unstimulated Jurkat cells and from three Jurkat-derived clones expressing V5-tagged UBASH3A (5E4, 1F6 and 2F5) were subjected to immunoblotting with anti-V5 and subsequently with anti-γ-tubulin after stripping. The asterisk indicates the monoubiquitinated form of V5-tagged UBASH3A. (**C**) Flow-cytometry analysis of CD3ε and TCR-Vβ8 on the plasma membrane of unstimulated Jurkat cells, and UBASH3A-overexpressing 1F6 and 2F5 cells. Data shown are representative of four independent experiments. (**D**) Flow-cytometry analysis of CD3ε and

TCR-Vβ8 on the plasma membrane of unstimulated Jurkat cells and UBASH3A$^{-/-}$ 2.1F7 cells. Data shown are representative of four independent experiments. (**E**) The median fluorescence intensities (MFI) of cell-surface CD3ε and TCR-Vβ8 on unstimulated Jurkat, UBASH3A$^{-/-}$ 2.1F7, and UBASH3A-overexpressing 2F5 cells are shown. The mean and SEM values are indicated by solid lines and error bars, respectively. The data are pooled from five independent experiments. *$p < 0.05$, **$p < 0.01$, ns: not significant (unpaired two-tailed Mann-Whitney U test).

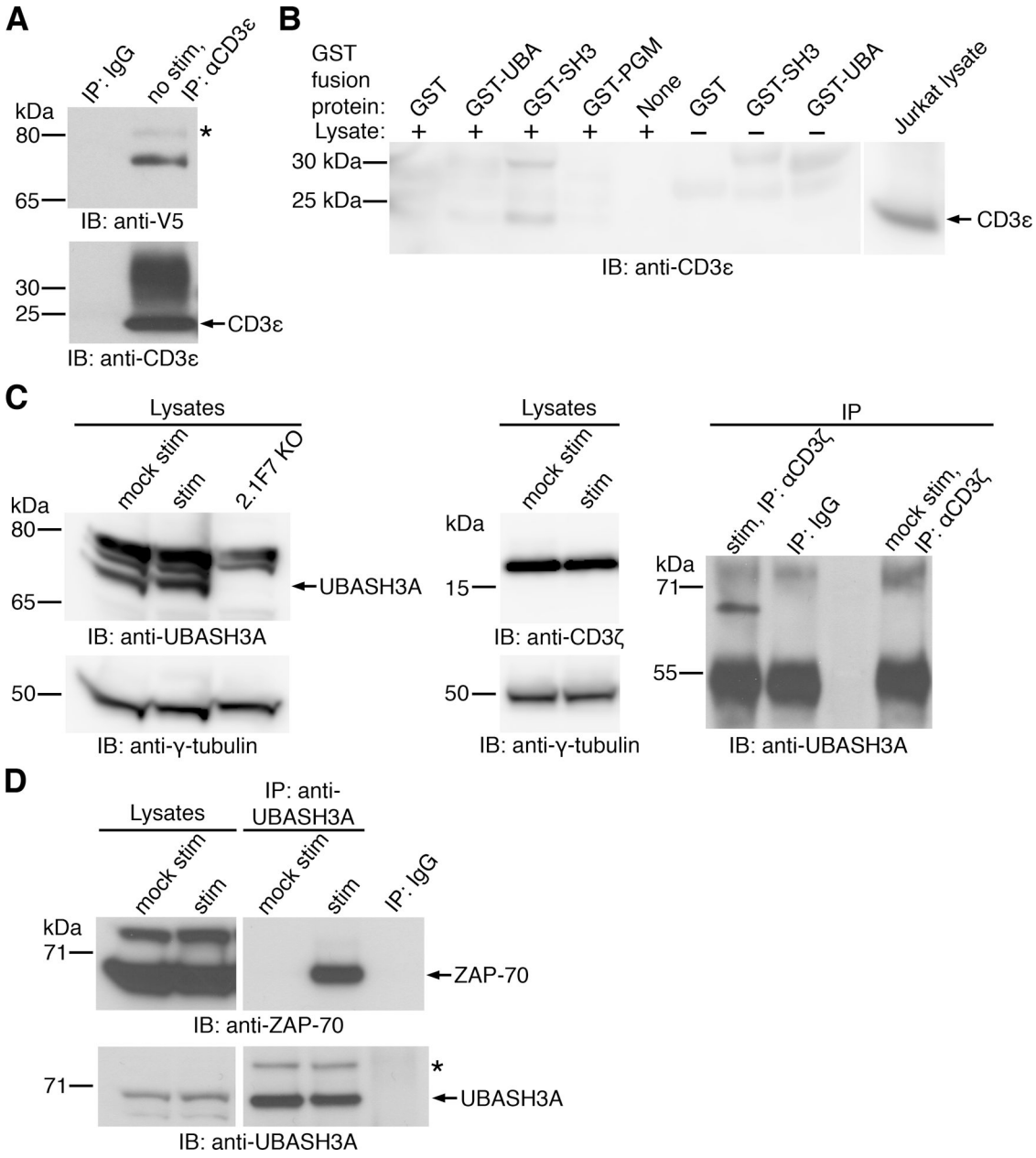

FIGURE 2.

UBASH3A interacts with CD3 chains and ZAP-70. (**A**) Lysate from unstimulated Jurkat cells expressing V5-tagged UBASH3A was immunoprecipitated with anti-CD3ε or IgG, and the immunoprecipitates were subjected to immunoblotting with anti-V5 and subsequently with anti-CD3ε after stripping. (**B**) GST pull-down assay using GST-tagged UBA, SH3 and PGM domains of UBASH3A with and without whole-cell lysate from unstimulated Jurkat cells. The pull-down products and the Jurkat lysate were subjected to immunoblotting with anti-CD3ε. (**C**) Lysates from mock-stimulated Jurkat cells, and from Jurkat cells stimulated with anti-CD3 and anti-CD28 antibodies for 3 min, were immunoprecipitated with anti-CD3ζ or IgG. The input lysates and lysate from unstimulated UBASH3A$^{-/-}$ 2.1F7 cells were subjected to immunoblotting with anti-UBASH3A or anti-CD3ζ, and subsequently with

anti-γ-tubulin after stripping. The immunoprecipitates were subjected to immunoblotting with anti-UBASH3A. (**D**) Lysates from mock-stimulated Jurkat cells, and from Jurkat cells stimulated with anti-CD3 and anti-CD28 antibodies for 3 min, were immunoprecipitated with anti-UBASH3A or IgG. The input lysates and the immunoprecipitates were subjected to immunoblotting with anti-ZAP-70 and subsequently with anti-UBASH3A after stripping. The blots in **A-D** are representative of two independent experiments. The asterisks indicate the monoubiquitinated form of UBASH3A.

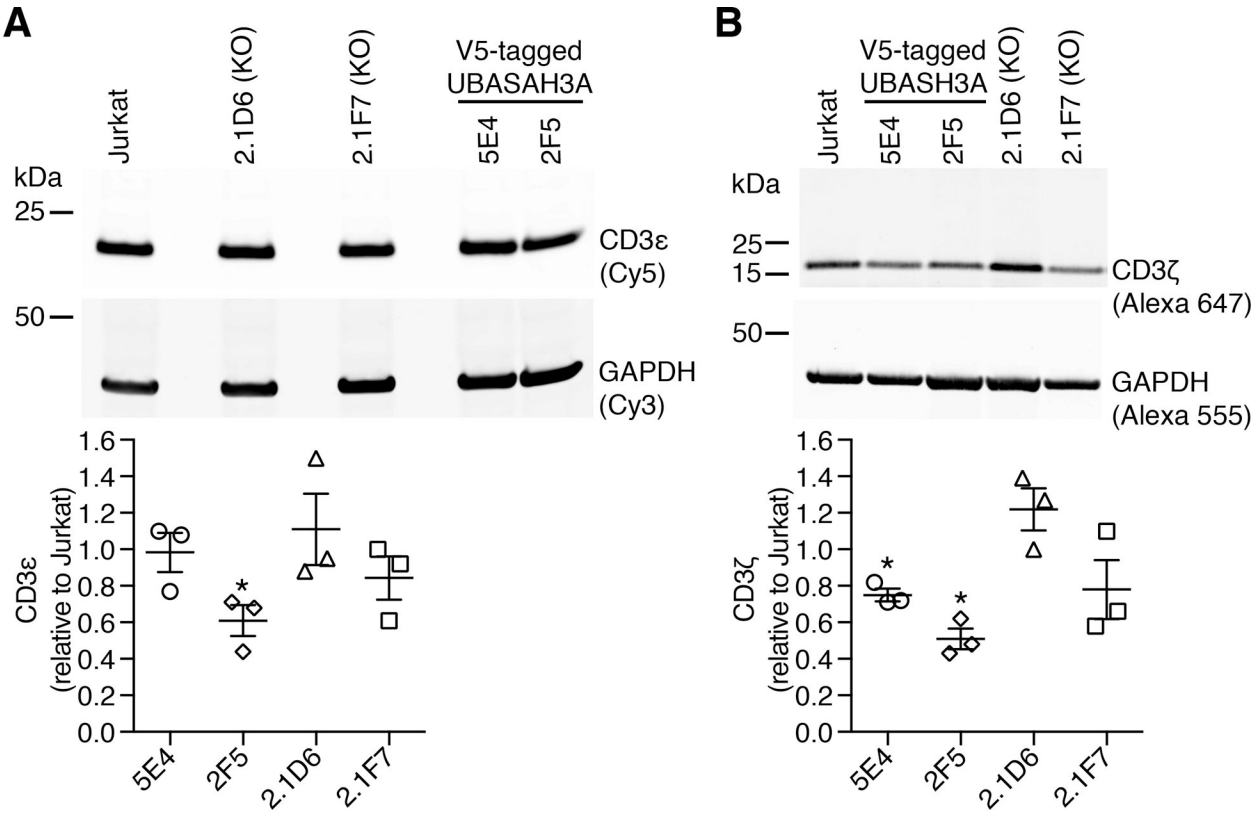

FIGURE 3.

Increased UBASH3A expression is associated with decreased amounts of total CD3ε and CD3ζ. (**A** and **B**) Whole-cell lysates from unstimulated Jurkat cells, and Jurkat-derived UBASH3A$^{-/-}$ (2.1D6 and 2.1F7) and UBASH3A-overexpressing (5E4 and 2F5) clones were subjected to multiplex fluorescent immunoblotting using the indicated combination of antibodies. The abundances of total CDε (**A**) and CD3ζ (**B**), relative to Jurkat cells, in UBASH3A$^{-/-}$ and UBASH3A-overexpressing clones are shown. The mean and SEM values are represented by solid lines and error bars, respectively. The data are pooled from three independent immunoblotting experiments for CDε, and three for CD3ζ. *$p < 0.05$ (unpaired two-tailed Student's t-test).

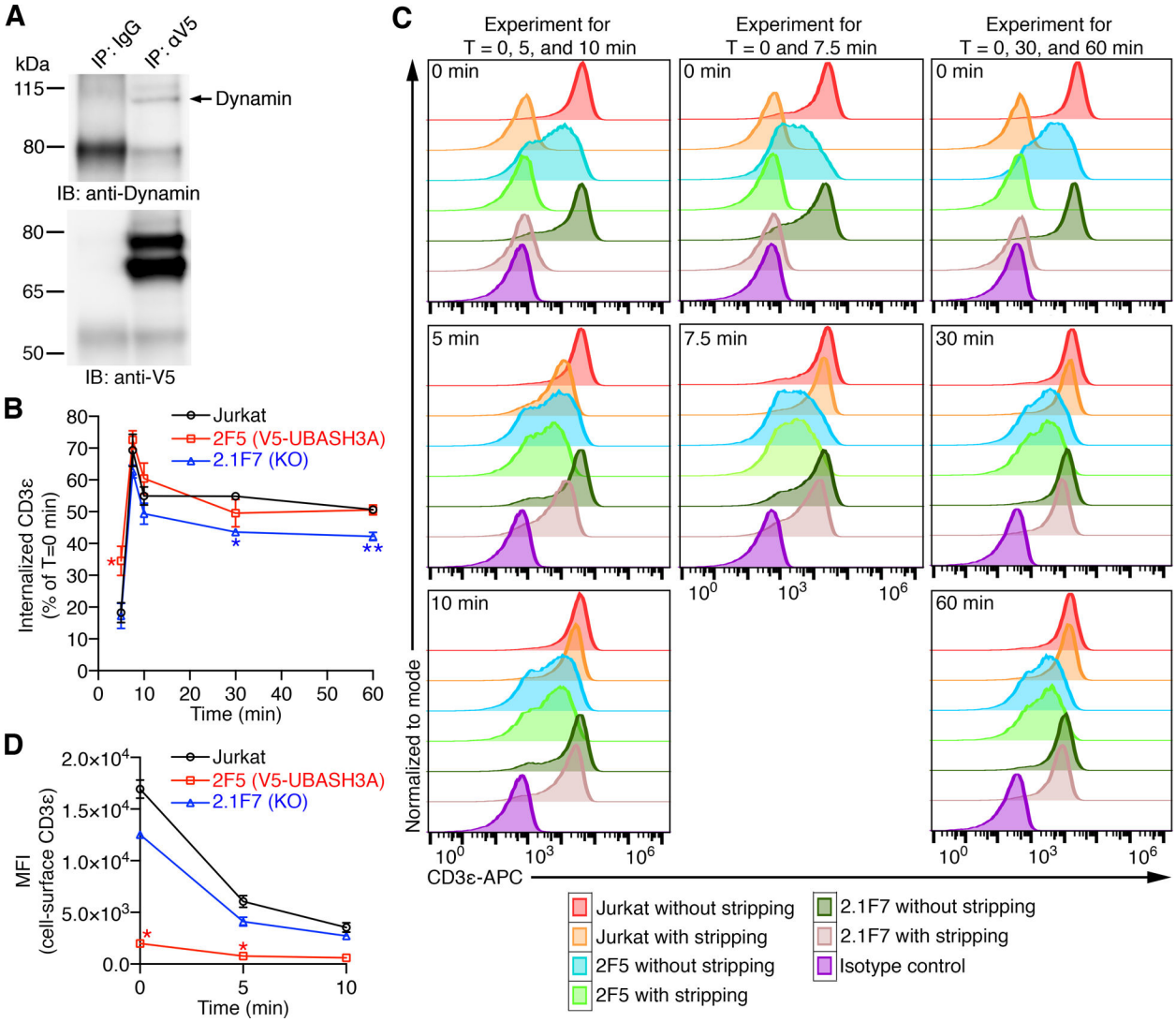

FIGURE 4.

UBASH3A binds to dynamin and affects the downmodulation of cell-surface TCR-CD3 upon TCR engagement. (**A**) Lysate from unstimulated Jurkat cells expressing V5-tagged UBASH3A was immunoprecipitated with anti-V5 or IgG, and the immunoprecipitates were subjected to immunoblotting with anti-dynamin and subsequently with anti-V5 after stripping. The blot shown is representative of two independent experiments. (**B**) Cell-surface CD3ε molecules were labeled with APC-conjugated anti-CD3ε antibodies. Unbound antibodies were washed off, and the cells were incubated at 37°C for the indicated periods of time. After the incubation, the antibodies bound to the cell-surface CD3ε were stripped, and then the amount of intracellular APC-conjugated anti-CD3ε antibodies was measured by flow cytometry. Jurkat cells, and Jurkat-derived UBASH3A$^{-/-}$ (2.1F7) and UBASH3A-overexpressing (2F5) cells were used in this assay. The average percentages of cell-surface CD3ε molecules at time 0 that have been internalized at the indicated time points are shown. The error bars represent SEM. The data are pooled from 13 independent experiments. *$p <$ 0.05, **$p < 0.005$ (Tukey's honest significance test following ANOVA; p values for

comparisons involving the Jurkat group at each time point are shown). (**C**) Representative histograms of CD3ε-APC and of APC-conjugated isotype controls from the experiments used in **B**. (**D**) Jurkat cells, UBASH3A$^{-/-}$ 2.1F7, and UBASH3A-overexpressing 2F5 cells were stimulated with 5 μg/mL of plate-bound anti-CD3 for 0, 5, and 10 min at 37°C, and then subjected to flow-cytometry analysis. The average values of median fluorescence intensities (MFI) of cell-surface CD3ε are shown. The error bars represent SEM. The data are pooled from three independent experiments. In contrast to the assay in **B** and **C** which specifically quantifies the internalization of cell-surface CD3ε in response to TCR-CD3 ligation, the assay in **D** reflects combined effects of ligation-triggered internalization of existing cell-surface CD3ε and arrival of new CD3ε molecules at the plasma membrane. *$p < 0.05$ (two-tailed Dunn's multiple comparison test following Kruskal-Wallis test; p values adjusted with the Benjamini-Hochberg method for comparisons involving the Jurkat group at each time point are shown).

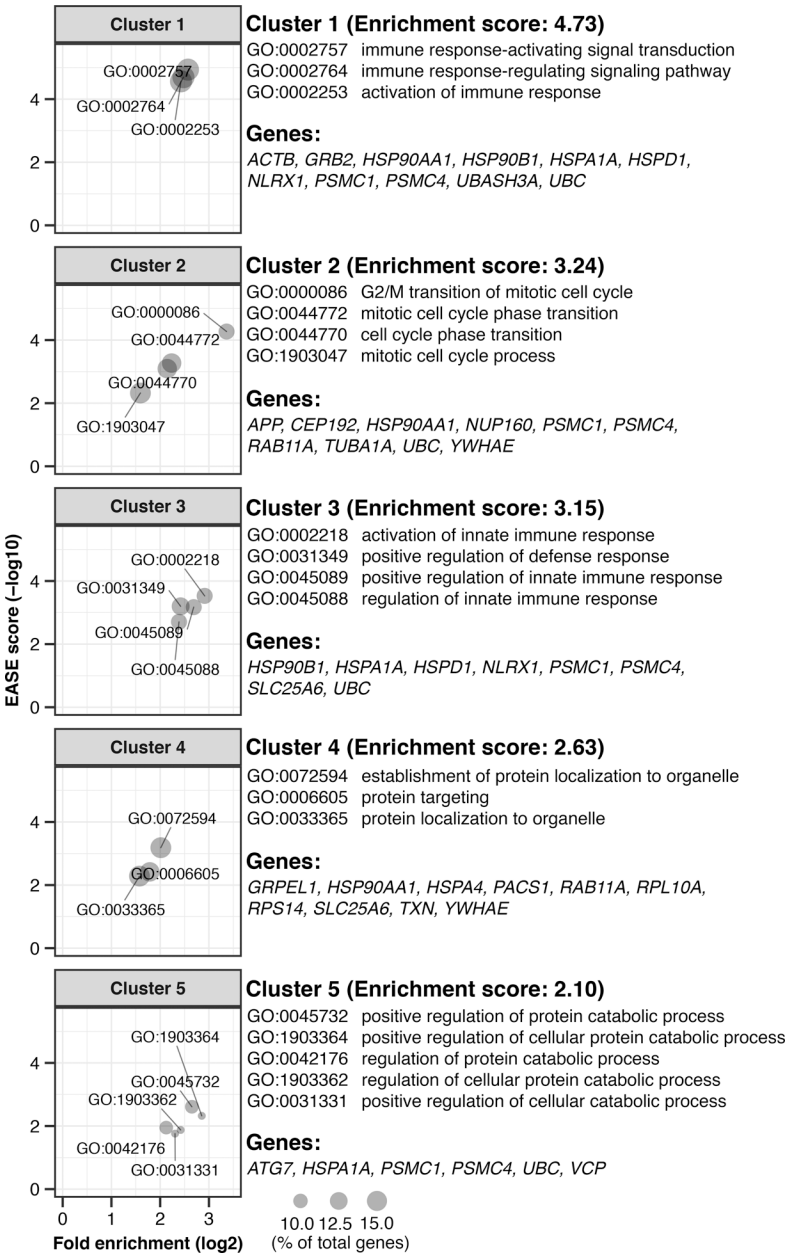

FIGURE 5.

Functional annotation clustering of gene ontology (GO) terms associated with UBASH3A-binding partners in Jurkat cells. The top five clusters identified by the DAVID program are shown. EASE score is the *p* value from DAVID's modified Fisher's exact test. Enrichment score is the geometric mean (in -log scale) of the *p* values of individual annotation terms in an annotation cluster, and higher enrichment score indicates higher biological significance. The size of each bubble on the bubble plots represents the percentage of total genes in a GO term that were identified as UBASH3A-binding partners.

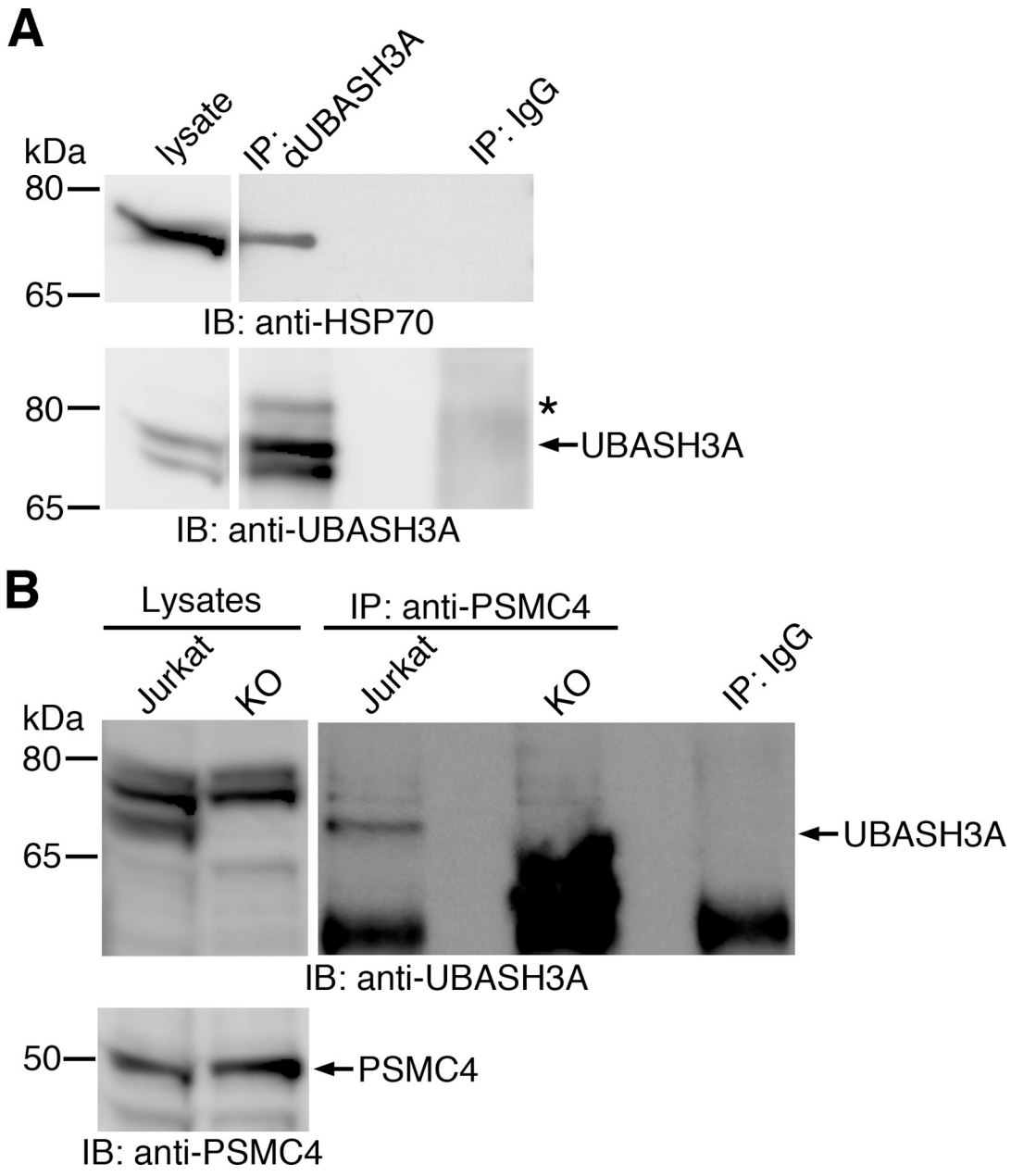

FIGURE 6.

UBASH3A interacts with HSP70 and PSMC4 in unstimulated Jurkat cells. (**A**) Lysate from unstimulated Jurkat was immunoprecipitated with anti-UBASH3A or IgG. The immunoprecipitates and the input lysate were subjected to immunoblotting with anti-HSP70 and subsequently with anti-UBASH3A after stripping. The asterisk indicates the monoubiquitinated form of UBASH3A. (**B**) Lysates from unstimulated Jurkat cells and Jurkat-derived UBASH3A$^{-/-}$ cells were immunoprecipitated with anti-PSMC4 or IgG. The immunoprecipitates and the input lysates were subjected to immunoblotting with anti-UBASH3A or anti-PSMC4. The blots in **A-B** are representative of two independent experiments.

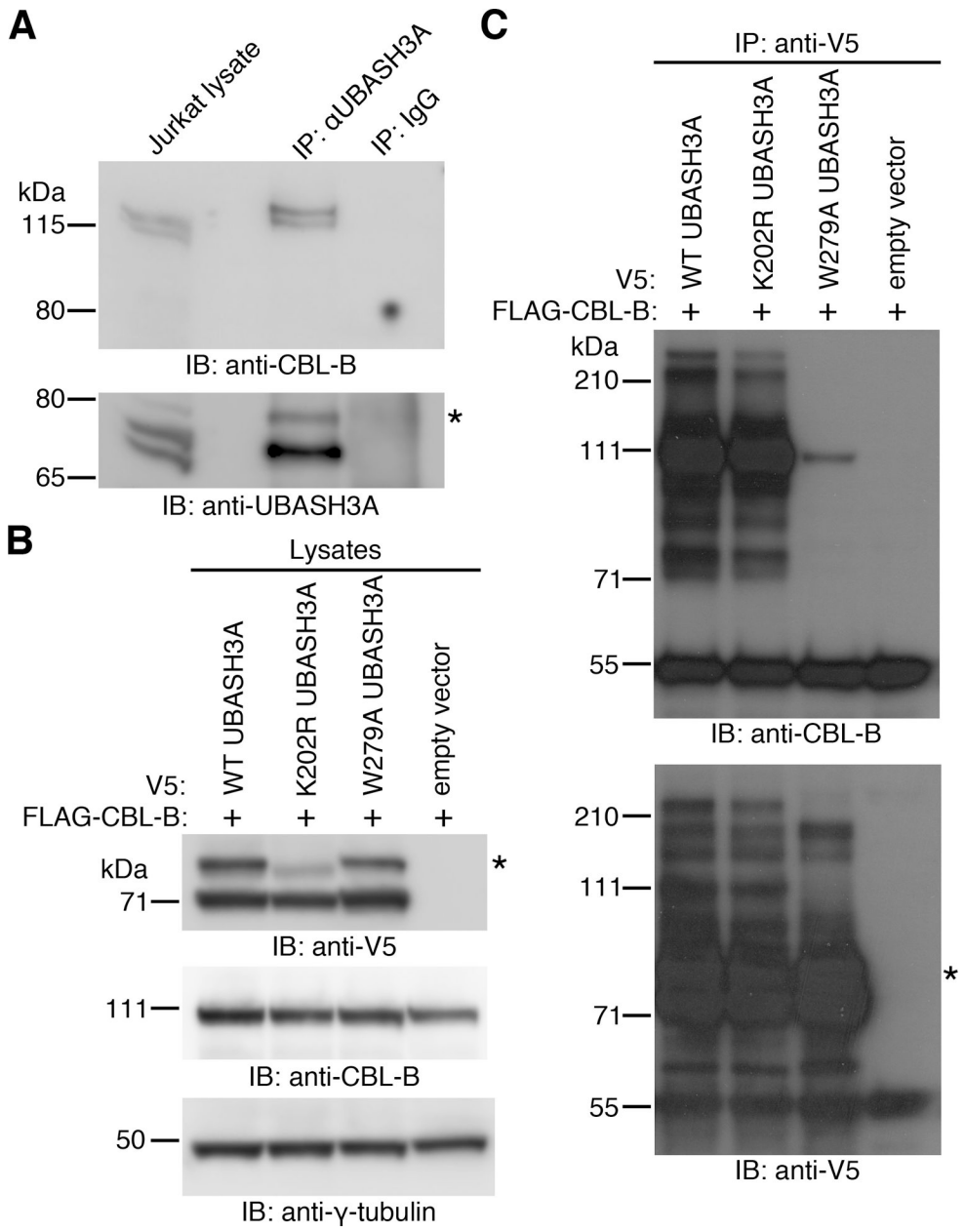

FIGURE 7.

UBASH3A binds to CBL-B via its SH3 domain. (**A**) Lysate from unstimulated Jurkat cells was immunoprecipitated with anti-UBASH3A or IgG. The immunoprecipitates and the input lysate were subjected to immunoblotting with anti-CBL-B and subsequently with anti-UBASH3A after stripping. (**B** and **C**) HEK293T cells were co-transfected with constructs encoding FLAG-tagged CBL-B, and the indicated form of V5-tagged UBASH3A—wild-type (WT), K202R (ubiquitination-site mutant) and W279A (SH3 mutant)—or V5. In **B**, lysates from the transfected cells were subjected to immunoblotting sequentially with anti-V5, anti-CBL-B, and anti-γ-tubulin. In **C**, the lysates were immunoprecipitated with anti-V5, and the immunoprecipitates were subjected to immunoblotting with anti-CBL-B and

subsequently with anti-V5 after stripping. The blots in **A**-**C** are representative of two independent experiments. The asterisks indicate the monoubiquitinated form of UBASH3A.

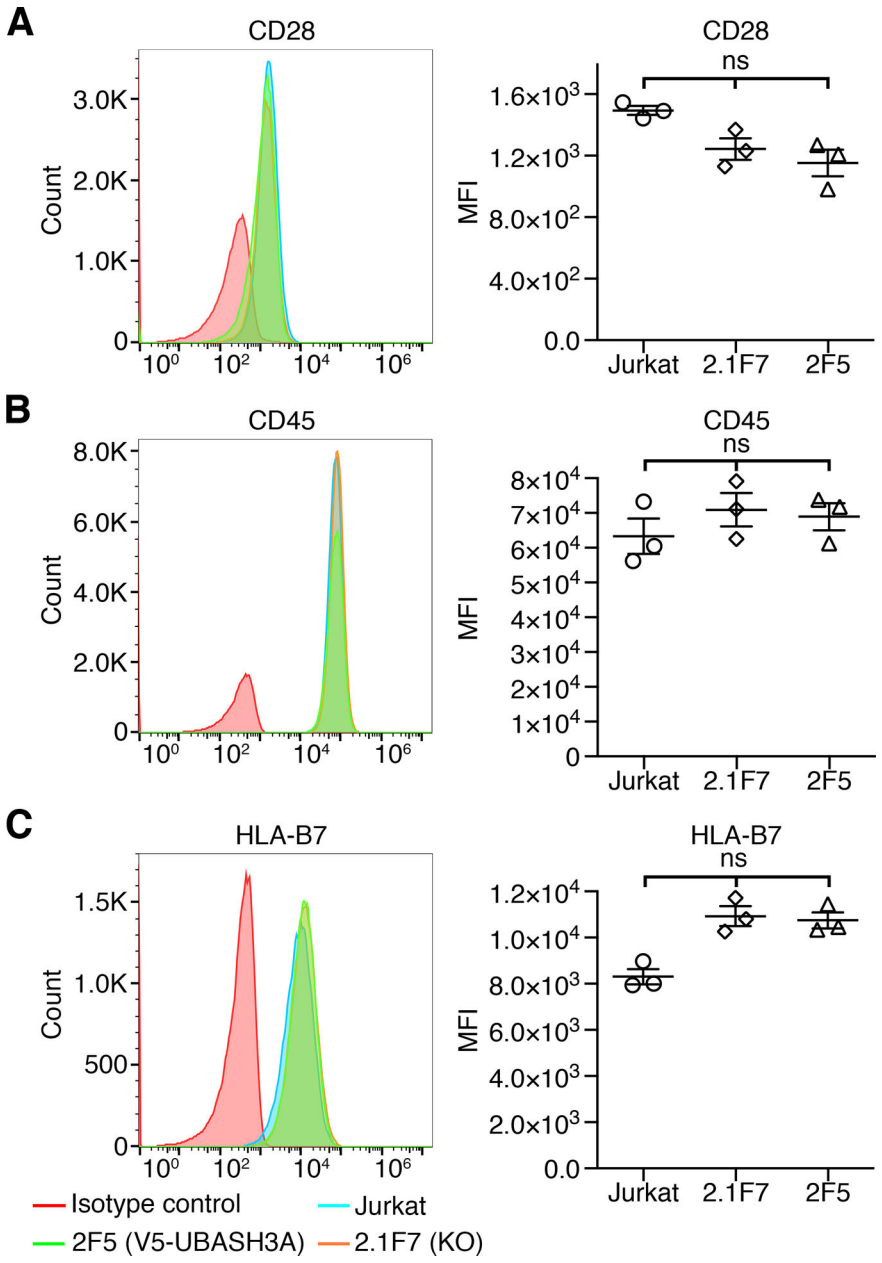

FIGURE 8.

UBASH3A does not affect the amounts of cell-surface CD28, CD45 and HLA-B7 in unstimulated T cells. (**A-C**) Flow-cytometry analysis of CD28, CD45 and HLA-B7 on the plasma membrane of unstimulated Jurkat cells, and Jurkat-derived UBASH3A$^{-/-}$ (2.1F7) and UBASH3A-overexpressing (2F5) cells. The histograms are representative of three independent experiments. The median fluorescence intensities (MFI) are shown. The mean and SEM values are indicated by solid lines and error bars, respectively. The data are pooled from three independent experiments for each of the membrane receptors. ns: not significant (Kruskal-Wallis test).